

A time-dependent generalized Floquet calculation of the laser-induced lineshape in attosecond transient absorption spectra

Xu-Han Wang(王旭涵), Di Zhao(赵迪), and Peng-Bo Li(李蓬勃)
Citation: Chin. Phys. B, 2025, 34 (**11**): 113201. DOI: 10.1088/1674-1056/ae07c0
http://cpb.iphy.ac.cn; http://iopscience.iop.org/cpb

What follows is a list of articles you may be interested in

Theoretical investigations of population trapping phenomena in atomic four-color, three-step photoionization scheme

Xiao-Yong Lu(卢肖勇) and Ya-Peng Sun(孙亚鹏)
Chin. Phys. B, 2024, 33 (**3**): 033202. DOI: 10.1088/1674-1056/ad10fc

Light-shift induced by two unbalanced spontaneous decay rates in EIT (CPT) spectroscopies under Ramsey pulse excitation

Xiaoyan Liu(刘晓艳), Xu Zhao(赵旭), Jianfang Sun(孙剑芳), Zhen Xu(徐震), and Zhengfeng Hu(胡正峰)
Chin. Phys. B, 2021, 30 (**8**): 083203. DOI: 10.1088/1674-1056/ac0528

Quantal studies of sodium 3p←3s photoabsorption spectra perturbed by ground lithium atoms

N Lamoudi, F Talbi, M T Bouazza, M Bouledroua, K Alioua
Chin. Phys. B, 2019, 28 (**6**): 063202. DOI: 10.1088/1674-1056/28/6/063202

The ac Stark shifts of the terahertz clock transitions of barium

Yu Geng-Hua (余庚华), Geng Ying-Ge (耿鹰鸽), Li Long (李隆), Zhou Chao (周超), Duan Cheng-Bo (段丞博), Chai Rui-Peng (柴瑞鹏), Yang Yong-Ming (杨永明)
Chin. Phys. B, 2015, 24 (**10**): 103201. DOI: 10.1088/1674-1056/24/10/103201

Theoretical study of amplified spontaneous emission intensity and bandwidth reduction in polymer

A. Hariri, S. Sarikhani
Chin. Phys. B, 2015, 24 (**4**): 043201. DOI: 10.1088/1674-1056/24/4/043201

A time-dependent generalized Floquet calculation of the laser-induced lineshape in attosecond transient absorption spectra

Xu-Han Wang(王旭涵), Di Zhao(赵迪)†, and Peng-Bo Li(李蓬勃)

Shaanxi Province Key Laboratory of Quantum Information and Quantum Optoelectronic Devices, School of Physics, Xi'an Jiaotong University, Xi'an 710049, *China*

(Received 22 July 2025; revised manuscript received 2 September 2025; accepted manuscript online 17 September 2025)

We introduce a time-dependent generalized Floquet (TDGF) approach to calculate attosecond transient absorption spectra of helium atoms subjected to the combination of an attosecond extreme ultraviolet (XUV) pulse and a delayed few-cycle infrared (IR) laser pulse. This TDGF approach provides a Floquet understanding of the laser-induced change of resonant absorption lineshape. It is analytically demonstrated that the phase shift of the time-dependent dipole moment that results in the lineshape changes consists of two components, the adiabatic laser-induced phase (LIP) due to the IR-induced Stark shifts of adiabatic Floquet states and the non-adiabatic phase correction due to the non-adiabatic IR-induced coupling between adiabatic Floquet states. Comparisons of the spectral lineshape calculated based on the TDGF approach with the results obtained with the LIP model [*Phys. Rev. A* **88** 033409 (2013)] and the rotating-wave approximation (RWA) are presented for several typical cases, demonstrating that TDGF universally and accurately captures IR-induced lineshape changes. It is suggested that the LIP model works as long as the generalized adiabatic theorem [*PRX Quantum* **2** 030302 (2021)] holds, and the RWA works when the higher-order IR-coupling effect in the formation of adiabatic Floquet states is neglectable.

Keywords: attosecond transient absorption spectra, Floquet analysis, non-adiabatic phase correction

PACS: 32.70.Jz, 42.50.Hz

DOI: 10.1088/1674-1056/ae07c0 **CSTR:** 32038.14.CPB.ae07c0

1. Introduction

In the past decades, the advent of attosecond pulses has offered a powerful tool to trace the electronic response in atoms, molecules and solid targets in the natural timescale of electronic dynamics.[1–33] An attosecond extreme ultraviolet (XUV) pulse synchronized with an infrared (IR) laser pulse gives rise to a transient absorption measurement, so-called attosecond transient absorption spectroscopy (ATAS), to investigate the IR-laser-driven electronic dynamics at the sub-optical-cycle scale, with the temporal resolution indirectly accessed through the highly controlled time delay between pulses. For atomic systems, typical features of ATA spectra include[34,35] light-induced states (LISs) and subcycle oscillating fringes when the XUV pulse arrives during the IR pulse, hyperbolic sidebands when the XUV pulse arrives before the IR pulse, and IR-induced change of resonant absorption lineshape for delays in which the XUV pulse precedes or overlaps with the IR pulse.

The Floquet theory has brought a conceptual picture of ATA process.[35] For instance, the LISs in ATA spectra are the Floquet states that are dipole allowed to the ground state, and the subcycle oscillations are the quantum beating between different Floquet states that collapse to the same bare state when the IR pulse turns off.[35–37] Yet the IR-induced change of resonant absorption lineshape has not been explored in the Floquet formalism. Ott *et al.*[10] and Chen *et al.*[38] propose a laser-induced phase (LIP) model under the lowest-order assumption, in which the laser-induced modification of the population of the XUV-excited bright state is neglected and only a laser-induced modification of the bright state phase is included. The phase shift of the bright state gives rise to a phase shift of the time-dependent dipole moment relative to the XUV-only case, resulting in the laser-induced lineshape changes in ATA spectra. Several potential applications, such as the reconstruction of laser-driven electronic dynamics[11,39] and the generation of XUV frequency combs,[40] have been proposed based on the LIP model. However, in the frame of the LIP model, neither the second order perturbation theory (SOPT) nor the rotating wave approximation (RWA) is a universal approach to accurately reproduce the IR-induced change of resonant absorption lineshape.[35]

In this paper, we introduce a time-dependent generalized Floquet (TDGF) approach to solve the time-dependent Schrödinger equation (TDSE) of XUV-excited helium atom driven by a delayed few-cycle IR pulse, and investigate the IR-induced lineshape change in ATA spectra in the picture of adiabatic Floquet states. By employing the generalized adiabatic theorem,[41] it is demonstrated that the lowest-order assumption in the LIP model is equivalent to the generalized adiabatic approximation (GAA) and the LIP is the dif-

†Corresponding author. E-mail: d.zhao@mail.xjtu.edu.cn

© 2025 Chinese Physical Society and IOP Publishing Ltd. All rights, including for text and data mining, AI training, and similar technologies, are reserved.

ference of dynamical phase shifts of adiabatic Floquet states. The total IR-coupling-induced phase shift imported on the time-dependent dipole moment consists of two parts, the adiabatic LIP due to the IR-induced stark shifts of adiabatic Floquet states and the non-adiabatic phase correction due to the IR-induced non-adiabatic coupling between adiabatic Floquet states. We present comparison of resonant absorption lineshape calculated based on the TDGF approach with those based on GAA and RWA in a He-like few-level model. It is suggested that the failure of LIP in the case of weak driving and small detuning is due to the non-ignorable IR-induced coupling between adiabatic Floquet states, i.e., the breakdown of generalized adiabatic theorem, while the failure of RWA in the case of strong driving and large detuning is due to the neglect of higher-order coupling in the formation of adiabatic Floquet states. Our numerical calculation also shows that the TDGF calculation of resonant absorption lineshape in a He-like few-level model agrees qualitatively with the *ab initio* calculation of single-active-electron (SAE) helium atom.

The paper is organized as follows. First, we briefly describe the single-atom response function for the calculation of ATA spectra and the LIP model in Subsection 2.1, derive the total laser-induced phase in the frame of generalized Floquet theory, and explore the LIP as the adiabatic limit of the total laser-induced phase by employing the generalized adiabatic approximation in Subsection 2.2. In Section 3, we present the investigation of IR-induced lineshape change via the comparison of calculated ATA spectra by employing different approaches, for the cases with weak driving and moderate detuning in Subsection 3.1, strong driving and large detuning in Subsection 3.2, and weak driving and small detuning in Subsection 3.3. Finally, in Section 3.4, we examine the efficiency of the TDGF approach via the comparison with the *ab initio* calculation of SAE helium atom. Summaries and concluding remanks are given in Section 4. Atomic units ($\hbar = e = m_e = a_0 = 1$) are used throughout, unless indicated otherwise.

2. Theory and methods

2.1. The single-atom response function and the LIP model

We consider a He-like three-level system driven by the combination of an attosecond XUV pulse and a few-cycle IR pulse. The $1s^2$, 1s2p and 1s2s states of helium atom are included and labelled as $|\alpha\rangle$, $|\beta\rangle$ and $|\gamma\rangle$, respectively, as shown in Fig. 1. The time-dependent wavefunction can be expanded as

$$\begin{aligned}|\Psi(t)\rangle \;=\; & C_\alpha(t)\,\mathrm{e}^{-\mathrm{i}\mathcal{E}^0_\alpha t}|\alpha\rangle + C_\beta(t)\,\mathrm{e}^{-\mathrm{i}\mathcal{E}^0_\beta t}|\beta\rangle \\ & + C_\gamma(t)\,\mathrm{e}^{-\mathrm{i}\mathcal{E}^0_\gamma t}|\gamma\rangle, \end{aligned} \tag{1}$$

in which $\mathcal{E}^0_\alpha$, $\mathcal{E}^0_\beta$ and $\mathcal{E}^0_\gamma$ are the eigenenergies of field-free states, and C_α, C_β and C_γ are the probability amplitudes of corresponding states. The time-dependent Hamiltonian is written as

$$\begin{aligned}\hat{H}(t) \;=\; & \hat{H}_0 + \hat{V}(t) \\ =\; & |\alpha\rangle\mathcal{E}^0_\alpha\langle\alpha| + |\beta\rangle\mathcal{E}^0_\beta\langle\beta| + |\gamma\rangle\mathcal{E}^0_\gamma\langle\gamma| \\ & - E^0_{\mathrm{X}}(t)\cos(\omega_{\mathrm{X}}t)(\mu^0_{\alpha\beta}|\alpha\rangle\langle\beta| + \mu^0_{\beta\alpha}|\beta\rangle\langle\alpha|) \\ & - E^0_{\mathrm{I}}(t-\tau)\cos(\omega_{\mathrm{I}}t - \omega_{\mathrm{I}}\tau) \\ & \times(\mu^0_{\beta\gamma}|\beta\rangle\langle\gamma| + \mu^0_{\gamma\beta}|\gamma\rangle\langle\beta|), \end{aligned} \tag{2}$$

in which $\mu^0_{\alpha\beta} = \mu^{0*}_{\beta\alpha} = e\langle\alpha|z|\beta\rangle$ and $\mu^0_{\beta\gamma} = \mu^{0*}_{\gamma\beta} = e\langle\beta|z|\gamma\rangle$ are the transition matrix elements, $\omega_{\mathrm{I(X)}}$ and $E^0_{\mathrm{I(X)}}(t)$ are the carrier frequency and pulse-envelope function of the IR (XUV) pulse, respectively, and the two pulses with the relative time delay τ are both polarized along the z axis. The XUV pulse couples the $|\alpha\rangle$ and $|\beta\rangle$ states, and the IR pulse only couples the $|\beta\rangle$ and $|\gamma\rangle$ states. The time-dependent dipole moment $d(t)$ is determined by

$$d(t) = C^*_\alpha(t)C_\beta(t)\mu^0_{\alpha\beta}\,\mathrm{e}^{-\mathrm{i}\omega_{\beta\alpha}t} + \mathrm{c.c.}, \tag{3}$$

where we only measure frequencies relative to the $|\alpha\rangle$ state, and $\omega_{\beta\alpha} = \mathcal{E}^0_\beta - \mathcal{E}^0_\alpha$. The coefficients $C_\alpha(t)$ and $C_\beta(t)$ can be obtained by numerically solving the TDSE with Hamiltonian (2) via the fourth-order Runge–Kutta (RK) method.

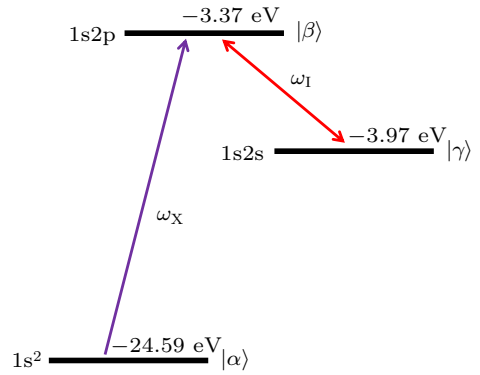


Fig. 1. The three-level diagram of the single-active-electron helium atom, driven by the broadband, isolated attosecond XUV pulse and the IR dressing pulse.

The dipole moment $d(t)$ that is initiated by the interaction with the XUV pulse freely oscillates after the radiation fields have passed, and it would decay due to collisional broadening or spontaneous decay. In order to include these experimental effects in our calculation, the dipole moment $d(t)$ is multiplied by a smoothly decaying function before the Fourier transformation:

$$W(t) = \begin{cases} \mathrm{e}^{-\frac{\Gamma}{2}(t)}, & t > 0, \\ 1, & t \le 0, \end{cases} \tag{4}$$

where Γ stands for the phenomenological decay rate. Then we have the Fourier transform of the time-dependent dipole moment $d(t)$,

$$\tilde{d}(\omega) = \mu^0_{\alpha\beta}\int_0^\infty C^*_\alpha(t)C_\beta(t)\,\mathrm{e}^{\mathrm{i}(\omega-\omega_{\beta\alpha})t}W(t)\,\mathrm{d}t, \tag{5}$$

and the absorption spectra can be expressed as the response function defined by[42]

$$S(\omega) = 2\mathrm{Im}[\tilde{d}(\omega)\tilde{E}^*(\omega)], \tag{6}$$

where $\tilde{E}(\omega)$ is the Fourier transform of the total laser field $E(t)$. Note that, although the complete description of transient absorption spectra must account for the reshaping of an XUV pulse during the propagation, the single-atom response yields similar results as the full calculation for the helium atom.[42,43]

Since the preceding attosecond XUV pulse can be approximated by a δ-function due to its short duration, the three-level system can be further simplified into a primitive two-level system involving only the $|\beta\rangle$ and $|\gamma\rangle$ states and the IR pulse arriving after the XUV pulse. The LIP model assumes that:[10,38] the IR laser field does not modify the amplitude of the 1s2p state, but only varies the 1s2p state energy and thus imposes the LIP

$$\theta^{\mathrm{L}}_{\beta\alpha}(t) = \int_0^t \mathrm{d}t'[\delta\mathcal{E}_\beta(t') - \delta\mathcal{E}_\alpha(t')] \tag{7}$$

on the dipole moment, with $\delta\mathcal{E}_\alpha(t)$ and $\delta\mathcal{E}_\beta(t)$ being the ac Stark shifts of $1s^2$ and 1s2p states, respectively. And the response function can be expressed as

$$S_{\mathrm{A}}(\omega) = 2\tilde{\varepsilon}_{\mathrm{X}}\mathrm{Im}[\tilde{d}_{\mathrm{A}}(\omega)] \tag{8}$$

by using the approximation that the broadband IAP spectral amplitude $\tilde{\varepsilon}_{\mathrm{X}}$ is real and constant around $(\mathcal{E}^0_\eta - \mathcal{E}^0_\alpha)$, with

$$\tilde{d}_{\mathrm{A}}(\omega) = \mathrm{i}a_{\mathrm{X}}\mu^0_{\beta\alpha}\int_0^\infty \mathrm{e}^{-\mathrm{i}\theta_{\mathrm{L}}(t)}\,\mathrm{e}^{\mathrm{i}(\omega-\omega_{\beta\alpha})t}W(t)\,\mathrm{d}t, \tag{9}$$

in which $C_\alpha(t) = 1$ is taken due to the weak XUV pulse and $C_\beta(t) = \mathrm{i}a_{\mathrm{X}}\mathrm{e}^{-\mathrm{i}\theta_{\mathrm{L}}(t)}$. To first order in the XUV field $a_{\mathrm{X}} = \mu^0_{\beta\alpha}E_{\mathrm{X}}\tau_{\mathrm{X}}$ is a real, time-independent constant, in which E_{X} is the XUV field strength, and τ_{X} is a characteristic time for the XUV pulse, assumed to be much shorter than the period of IR field. The LIP gives rise to the laser-induced lineshape changes in ATA spectra.

2.2. The nonadiabatic phase correction to the LIP

To explore the IR-induced change of resonant absorption lineshape in the frame of Floquet theory, it is essential to investigate the IR-pulse-driven dynamics and the phase shift of the time-dependent dipole moment in terms of Floquet states. The generalized adiabatic theorem indicates that[41] Floquet states rather than energy eigenstates are preserved when the quantum system is driven by a modulated periodic field, such as an IR pulse in our work. Therefore, proceeding through a similar path as Ref. [41], we introduce a time-dependent generalized Floquet (TDGF) approach to solve the exact time evolution of the IR-pulse-driven system in the instantaneous Floquet basis $|\lambda(t;E_t)\rangle$,

$$|\Psi(t)\rangle = \sum_\lambda a_\lambda(t)\,\mathrm{e}^{-\mathrm{i}\theta_\lambda(t;E_t)}|\lambda(t;E_t)\rangle, \tag{10}$$

where $\theta_\lambda(t;E_t) \equiv \int_0^t \mathrm{d}t'\mathcal{E}_\lambda(t';E_{t'})$ is the dynamical phase, $\mathcal{E}_\lambda(t;E_t)$ is the instantaneous Floquet quasienergy, and $E_t = E^0_{\mathrm{I}}(t)$ labels the time-dependent amplitude of the IR pulse. For each value of E_t, the Hamiltonian is periodic and the instantaneous Floquet states can be defined as

$$|\psi_\lambda(t;E_t)\rangle = \mathrm{e}^{-\mathrm{i}\theta_\lambda(t;E_t)}|\lambda(t;E_t)\rangle. \tag{11}$$

The instantaneous Floquet quasienergy $\mathcal{E}_\lambda(t;E_t)$ and corresponding Floquet basis $|\lambda(t;E_t)\rangle$ satisfy the eigenvalue equation

$$\hat{H}_{\mathrm{F}}(t;E_t)|\lambda(t;E_t)\rangle = \mathcal{E}_\lambda(t;E_t)|\lambda(t;E_t)\rangle, \tag{12}$$

with the Floquet Hamiltonian $\hat{H}_{\mathrm{F}}(t;E_t) \equiv \hat{H}(t;E_t) - \mathrm{i}\partial/\partial t$.

Since the applied IR pulse is not strong enough to couple the ground state, the three-level model can be reduced into a two-level system including the upper two levels and the IR pulse. Substituting Eq. (10) into the two-level TDSE, $\mathrm{i}\partial/\partial t|\psi(t)\rangle = \hat{H}_{2\mathrm{l}}(t)|\psi(t)\rangle$, with the two-level Hamiltonian being

$$\begin{aligned}\hat{H}_{2\mathrm{l}}(t) \;=\; & |\beta\rangle\mathcal{E}^0_\beta\langle\beta| + |\gamma\rangle\mathcal{E}^0_\gamma\langle\gamma| - E^0_{\mathrm{I}}(t-\tau)\cos(\omega_{\mathrm{I}}t - \omega_{\mathrm{I}}\tau) \\ & \times(\mu^0_{\beta\gamma}|\beta\rangle\langle\gamma| + \mu^0_{\gamma\beta}|\gamma\rangle\langle\beta|),\end{aligned} \tag{13}$$

we obtain

$$\begin{aligned}&\sum_\lambda\left(\dot{a}_\lambda(t)|\lambda(t;E_t)\rangle + a_\lambda(t)\dot{E}_t\frac{\partial}{\partial E_t}|\lambda(t;E_t)\rangle\right) \\ &\times\mathrm{e}^{-\mathrm{i}\theta_\lambda(t;E_t)} = 0.\end{aligned} \tag{14}$$

Projecting onto an $|\lambda'(t;E_t)\rangle$ yields equations of motion for the coefficients

$$\begin{aligned}\dot{a}_{\lambda'}(t) \;=\; & -a_{\lambda'}(t)\dot{E}_t\langle\lambda'|\frac{\partial}{\partial E_t}|\lambda'\rangle \\ & + \sum_{\lambda\neq\lambda'} a_\lambda(t)\dot{E}_t\frac{\langle\lambda'|\partial\hat{H}_{\mathrm{F}}/\partial E_t|\lambda\rangle\,\mathrm{e}^{-\mathrm{i}(\theta_\lambda-\theta_{\lambda'})}}{\mathcal{E}_{\lambda'} - \mathcal{E}_\lambda},\end{aligned} \tag{15}$$

in which $\langle\lambda'|\partial/\partial E_t|\lambda\rangle = \langle\lambda'|\partial\hat{H}_{\mathrm{F}}/\partial E_t|\lambda\rangle/(\mathcal{E}_\lambda - \mathcal{E}_{\lambda'})$ is obtained by differentiating Eq. (12) with respect to E_t, and the t and E_t dependence is suppressed for brevity. The first term on the right side of Eq. (15) is the Berry connections of the instantaneous Floquet states, and the second term describes the diabatic transitions between the instantaneous Floquet states. The time-dependent dipole moment related to the state $|\alpha\rangle \approx |\lambda_\alpha\rangle$ can be written as

$$\begin{aligned}d(t) \;=\; & a^*_\alpha(t)\sum_\eta a_\eta(t)\langle\lambda_\alpha|\hat{z}|\lambda_\eta\rangle\,\mathrm{e}^{-\mathrm{i}(\theta_\eta-\theta_\alpha)} + \mathrm{c.c.} \\ =\; & \sum_\eta a_\eta(t)\mu_{\alpha\eta}\,\mathrm{e}^{-\mathrm{i}\theta^{\mathrm{d}}_{\eta\alpha}(t)}\,\mathrm{e}^{-\mathrm{i}\omega_{\eta\alpha}t} + \mathrm{c.c.},\end{aligned} \tag{16}$$

in which $\theta^{\rm d}_{\eta\alpha}(t)=\int_0^t {\rm d}t'[\delta\mathcal{E}_\eta(t')-\delta\mathcal{E}_\alpha(t')]$, $\mu_{\alpha\eta}=\langle\lambda_\alpha|\hat{z}|\lambda_\eta\rangle$ is the time-dependent transition matrix element between instantaneous Floquet states, and $a^*_\alpha(t)=1$ is taken due to the weak XUV pulse. The amplitude $a_\eta(t)$ can be recasted as

$$a_\eta(t)={\rm i}a^\delta_\eta(t)\,{\rm e}^{-{\rm i}\theta^\delta_\eta(t)}, \tag{17}$$

with real time-dependent variables $a^\delta_\eta(t)$ and $\theta^\delta_\eta(t)$ decomposing the effect of the IR driving field on the Floquet state $|\lambda_\eta\rangle$ into the time-dependent population modulation $a^\delta_\eta(t)$ and the phase deviation $\theta^\delta_\eta(t)$. $a^\delta_\eta(t)$ and $\theta^\delta_\eta(t)$ can be obtained by solving Eq. (15), with the initial condition of $a_\eta(t=0)={\rm i}a^\eta_{\rm X}$, where $a^\eta_{\rm X}=\mu^0_{\eta\alpha}E_{\rm X}\tau_{\rm X}$, and $\mu^0_{\eta\alpha}=e\langle\alpha|z|\eta\rangle$ is the transition matrix element between the ground state $|\alpha\rangle$ and an instantaneous Floquet state $|\lambda_\eta\rangle$. Then the response function in the instantaneous Floquet state formalism can be expressed as

$$S_{\rm F}(\omega)=2\tilde{\varepsilon}_{\rm X}{\rm Im}[\tilde{d}_{\rm F}(\omega)] \tag{18}$$

with

$$\tilde{d}_{\rm F}(\omega)={\rm i}\sum_\eta\int_0^\infty a^\delta_\eta(t)\mu_{\alpha\eta}\,{\rm e}^{-{\rm i}\theta^{\rm T}_\eta(t)}\,{\rm e}^{{\rm i}[\omega-\omega_{\eta\alpha})]t}W(t)\,{\rm d}t \tag{19}$$

in which

$$\theta^{\rm T}_\eta(t)=\theta^\delta_\eta(t)+\theta^{\rm d}_{\eta\alpha}(t) \tag{20}$$

is the total laser-induced phase imposed on the time-dependent dipole moment.

The response function in the frame of Floquet theory, Eqs. (18) and (19), contains the result in the LIP model, Eqs. (8) and (9), in the limit of the GAA.[41] If E_t changes much more slowly than the difference in Floquet quasienergies, the slow modulation will not cross-couple the Floquet states, and the second term on the right of Eq. (15) can be ignored. Then one can obtain $a_\eta(t)\approx{\rm i}a_{\rm X}$ and $\theta^{\rm T}_\eta(t)\approx\theta^{\rm d}_\eta(t)=\theta^{\rm L}_\eta(t)$. It is equivalent to the assumption of the LIP model,[38] and Eqs. (18)–(20) are reduced to Eqs. (7)–(9). The LIP $\theta^{\rm L}_\eta(t)$ is just the adiabatic limit of the total laser-induced phase, and it makes sense to refer $\theta^\delta_\eta(t)$ as the non-adiabatic phase correction to the adiabatic LIP. It is also worth mentioning that, under the GAA, the expression of dipole moment Eq. (16) can be reduced to the adiabatic Floquet dipole that has been employed to reproduce LISs and subcycle oscillation features in ATA spectra.[35]

In general, the non-adiabatic phase correction $\theta^\delta_\eta(t)$ cannot be obtained from Eq. (15) analytically, but it can be obtained numerically with the help of the solution of the time-independent generalized Floquet eigenvalue equations. It is expedient to enumerate the Floquet quasienergy vectors as $|\eta,l\rangle=|\eta\rangle\bigotimes|l\rangle$, with $|\eta\rangle$ being the system index and $|l\rangle$ being the Fourier vectors. For each instant, we can write the time-independent generalized Floquet matrix eigenvalue equation as[44]

$$\begin{aligned}&\sum_\eta\sum_{l'}\langle\kappa,l|\hat{H}_{\rm F}(t;E_t)|\eta,l'\rangle\langle\eta,l'|\lambda(t;E_t)\rangle\\&=\mathcal{E}_\lambda(t;E_t)\langle\kappa,l|\lambda(t;E_t)\rangle.\end{aligned} \tag{21}$$

In this paper, we set $|l,l'|\le 20$ to ensure the Floquet calculation is accessible and convergent. After solving the eigenvalue problem, we can obtain a set of quasienergy eigenvalues $\mathcal{E}_{\eta,l}(t;E_t)$ and corresponding eigenstates $|\lambda_{\eta,l}(t;E_t)\rangle$. Substituting the eigensolutions of each instant into Eq. (15), one can numerically solve the equations of motion for the coefficients in Eq. (15), obtain $a^\delta_\eta(t)$ and $\theta^\delta_\eta(t)$, and calculate the response function without any approximation.

3. Results and discussion

In this section, we numerically calculate the ATA spectra of a He-like three-level system by employing the TDGF approach as shown in Fig. 2. The TDGF method accurately transforms the bare-state basis in TDSE-RK method into the basis of instantaneous Floquet states without introducing any approximations, thus producing exactly the same ATAS spectra as the TDSE-RK method, which is shown in Fig. 2(b). The feature centered around 21.2 eV (marked with red solid line) is called a dressed bright state and the feature around 21.4 eV (marked with white solid lines) is called LIS, while the features around 19.6 eV, 22.7 eV (marked with red dashed lines) and the features around 19.8 eV, 23.0 eV (marked with white dashed lines) are called oscillating fringes.[34,35] In the frame of Floquet theory, a new interpretation of the LIS features is given: the feature marked with white solid line in Fig. 2 is from the dressed state of an atomic bare state, i.e., the instantaneous Floquet states $|\lambda_{\gamma,1}\rangle$, with the features marked with white dashed lines being the spectral consequences of two Floquet vectors $|\gamma,3\rangle$ and $|\gamma,-1\rangle$ among the expanding set $\sum_{\eta,l}\langle\eta,l|\lambda_{\gamma,1}\rangle$. As discussed in Ref. [35], the RWA can reproduce the main spectral peak of the dressed bright state and LIS, while the SOPT calculation could be viewed as a complement to it for explaining the laser-driven sub-cycle oscillating fringes. While the Floquet formalism is a powerful tool that provides a new conceptual picture for understanding ATAS features, a quantitative description of IR-induced lineshape changes remains lacking.

The spectral line near the $1s^2$–$1s2p$ resonant absorption peak, which corresponds to the time-dependent dipole moment between instantaneous Floquet states $|\lambda_\alpha\rangle$ and $|\lambda_{\beta,0}\rangle$

$$d_{\beta,0}(t)=a_{\beta,0}(t)\mu_{\alpha\beta}\,{\rm e}^{-{\rm i}\theta^{\rm d}_{\beta\alpha}(t)}\,{\rm e}^{-{\rm i}\omega_{\beta\alpha}}+{\rm c.c.}, \tag{22}$$

is taken as an example to investigate the laser-induced lineshape change via the comparison with the results based on the adiabatic LIP model and RWA. Here we restrict our discussion to the situation that the XUV pulse precedes and does not

overlap with the IR pulse. The coefficient $a_{\beta,0}(t)$ is obtained by numerically solving Eq. (15) with the initial condition

$$a_{\eta,l}(t=0)=\begin{cases} \mathrm{i}a_{\mathrm{X}}, & \text{for} \quad \eta=\beta \text{ and } l=0, \\ 0, & \text{others}, \end{cases} \tag{23}$$

and a_{X} being a real, time-independent constant. Note that, for the situation that the XUV pulse overlaps with the IR pulse, more Floquet states are initiated owing to multiphoton excitation, and the interference between multiphoton excitation paths would also introduce an additional phase factor onto the time-dependent dipole moment.

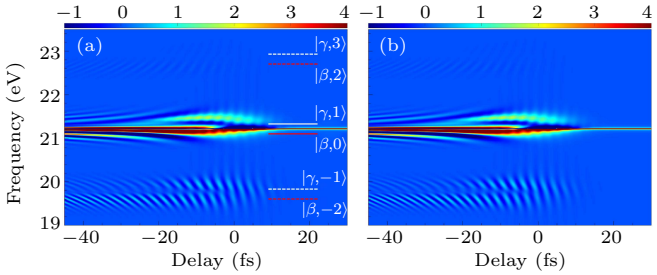


Fig. 2. The ATA spectra as a function of the time delay τ between the two pulses calculated by (a) TDGF and (b) TDSE-RK method. An IR pulse with 0.77 eV frequency, 1×10^{12} W/cm^2 peak intensity and 15 fs pulse width and an XUV pulse with 25 eV frequency, 1×10^{10} W/cm^2 peak intensity and 330 as pulse width are used in the calculation. The short lines represent main features of the spectra, of which the corresponding Floquet vectors are listed on the right.

The results based on the adiabatic LIP model are obtained by using Eqs. (8) and (9). While the results based on the RWA are obtained from the first-order Floquet calculation, since the rotating-wave terms are dropped in the first-order Floquet theory.[35] The parameters of the He-like three-level system are obtained via the diagonalization of the field-free Hamiltonian within the single-active-electron (SAE) approximation by employing the generalized pseudospectral method (see Appendix A for details), which gives $\mathcal{E}^0_\alpha=-0.90369$ a.u. (-24.59 eV), $\mathcal{E}^0_\beta=-0.12384$ a.u. (-3.37 eV), $\mathcal{E}^0_\gamma=-0.14589$ a.u. (-3.97 eV), $\mu_{\alpha\beta}=0.2084$ a.u., and $\mu_{\beta\gamma}=2.9471$ a.u. A 330 as-FWHM Gaussian XUV pulse with carrier frequency $\omega_{\mathrm{X}}=25$ eV and peak intensity 1×10^{10} W·cm^{-2} and a 40 fs-delayed 15 fs-FWHM Gaussian IR pulse are employed. The decay rate Γ is set as 5×10^{-3} eV. The carrier frequency and peak intensity of the IR pulse are chosen for the following specific cases.

3.1. Weak driving and moderate detuning

In the case of weak driving and moderate detuning, we set the peak intensity of the IR pulse $I_{\mathrm{IR}}=1\times10^{12}$ W/cm^2 and carrier frequency $\omega_{\mathrm{I}}=0.77$ eV. The probability amplitude of the Floquet quasienergy state $|\lambda_{\beta,0}\rangle$ is calculated by employing the TDGF approach. In Fig. 3(a), we plot the normalized population $|a^{\delta}_{\beta,0}(t)|^2$ (black-solid line), the LIP $\theta^{\mathrm{L}}_{\beta,0}(t)$ (red-dotted line) and the non-adiabatic phase correction $\theta^{\delta}_{\beta,0}(t)$ (blue-dash line) as a function of time. The population of $|\lambda_{\beta,0}\rangle$ is modulated due to the IR-induced cross-coupling with other adiabatic Floquet states, while $\theta^{\mathrm{L}}_{\beta,0}(t)$ and $\theta^{\delta}_{\beta,0}(t)$ are accumulated during the IR–atom interaction. $|a^{\delta}_{\beta,0}(t)|^2\approx1$ implies that the IR-induced coupling between $|\lambda_{\beta,0}\rangle$ and other adiabatic Floquet states can be ignored, and $\theta^{\delta}_{\beta,0}(t)\ll\theta^{\mathrm{L}}_{\beta,0}(t)$ leads to $\theta^{\delta}_{\beta,0}(t)\approx0$. In other words, the GAA is a good approximation. It is reasonable to consider the evolution of $|\lambda_{\beta,0}\rangle$ adiabatically, so one might expect the TDGF calculation would agree well with the TDSE-RK calculation with Eq. (6). Meanwhile the GAA indicates that the resonant absorption lineshape based on the adiabatic LIP model would agree well with that based on the TDGF approach. Indeed, in Fig. 3(d) we see good agreement of the TDGF calculation with the TDSE-RK calculation, as well as with the adiabatic LIP model. Figure 3(d) also presents the result obtained by the RWA that fits with the above three calculations well, implying that the contribution of the rotating-wave terms, i.e., the higher-order Floquet quasienergy vectors, are neglectable in the adiabatic Floquet state $|\lambda_{\beta,0}\rangle$.

3.2. Strong driving and large detuning

In the case of strong driving and large detuning, we set $I_{\mathrm{IR}}=5\times10^{13}$ W/cm^2 and $\omega_{\mathrm{I}}=1.55$ eV. In Fig. 3(b), we plot the normalized population $|a^{\delta}_{\beta,0}(t)|^2$ (black-solid line), the LIP $\theta^{\mathrm{L}}_{\beta,0}(t)$ (red-dotted line) and the non-adiabatic phase correction $\theta^{\delta}_{\beta,0}(t)$ (blue-dash line), as a function of time. Similar to the case of weak driving and moderate detuning, $|\lambda_{\beta,0}\rangle$ evolves adiabatically and the GAA is a good approximation. Figure 3(e) shows that, as expected, the TDGF approach and the adiabatic LIP model agree well with the TDSE-RK calculation. However, the RWA fails to reproduce the laser-induced change of the resonant absorption lineshape. As $\theta^{\delta}_{\beta,0}(t)\ll\theta^{\mathrm{L}}_{\beta,0}(t)$, the reasonable explanation is that the adiabatic LIP imported on the time-dependent dipole moment can not be calculated accurately by the RWA. We plot the LIPs after the IR driving pulse as a function of the peak intensity in Fig. 4. It is shown that the weaker the peak intensity of the IR driving pulse is, the better the LIP calculated by the RWA agrees with that calculated by the TDGF approach. It is easy to conclude that the breakdown of RWA is due to the dropped rotating-wave terms. This can be understood in the frame of adiabatic Floquet states. As the driving gets stronger, higher-order Floquet quasienergy vectors are coupled in the formation of the adiabatic Floquet state $|\lambda_{\beta,0}\rangle$. As a result, the RWA, i.e., the 'first-order' Floquet calculation, cannot give the convergent adiabatic Floquet states and their eigenenergies, leading to incorrect LIP obtained at higher peak intensity of the IR pulse.

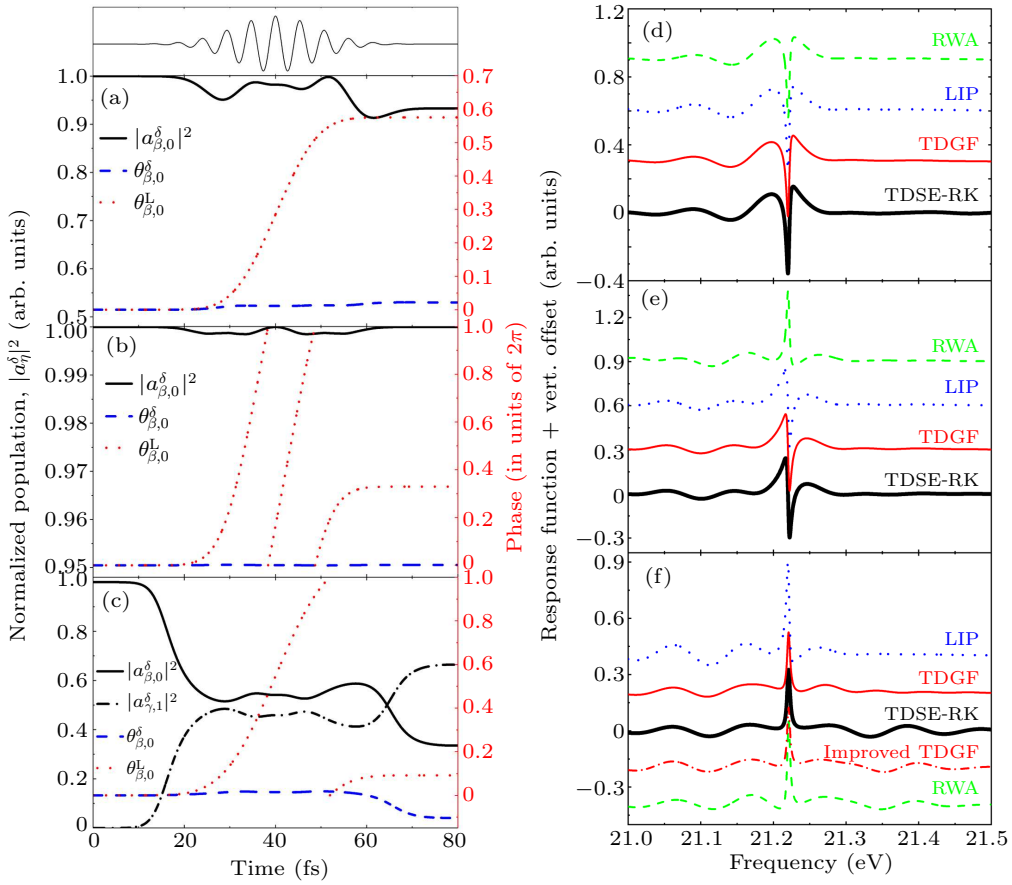


Fig. 3. The evolution of the Floquet quasienergy state $|\lambda_{\beta,0}(t)\rangle$ based on the TDGF approach is presented for the cases of (a) weak driving and moderate detuning, (b) strong driving and large detuning, and (c) weak driving and small detuning. The normalized population $|a^\delta_{\beta,0}|^2$ is represented with the black-solid line. The adiabatic LIP and the non-adiabatic phase correction are represented with the red-dotted and blue-dash lines, respectively. In (c), the normalized population $|a^\delta_{\gamma,1}|^2$ is represented with a black-dash-dotted line. The top panel illustrates the IR pulse centered at $\tau = 40$ fs. The response functions calculated from different approaches are shown in the region of the $1s^2$–$1s2p$ resonant absorption peak for the cases of (d) weak driving and moderate detuning, (e) strong driving and large detuning, and (f) weak driving and small detuning. The black-thick-solid, red-thin-solid, blue-dotted and green-dash lines are based on the numerical RK-method, the TDGF approach, the LIP model and the RWA, respectively. In (f), the red-dash-dotted line is based on the improved TDGF approach.

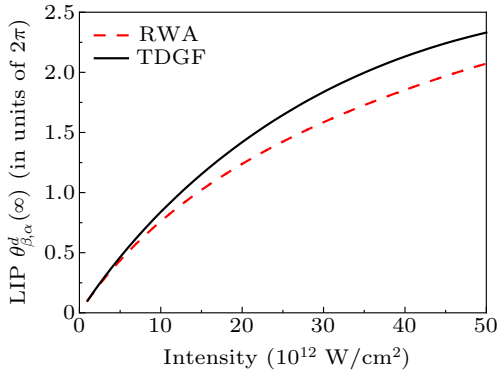


Fig. 4. The dependence of the LIP on the driving field intensity calculated from the RWA (black-solid line) and the TDGF approach (red-dotted line), respectively, in the case of large detuning $\omega_I = 1.55$ eV.

3.3. Weak driving and small detuning

In the case of weak driving and small detuning, we set $I_{IR} = 1 \times 10^{12}$ W/cm^2 and $\omega_I = 0.61$ eV. We plot the normalized population $|a^\delta_{\beta,0}(t)|^2$ (black-solid line), the LIP $\theta^L_{\beta,0}(t)$ (red-dotted line) and the non-adiabatic phase correction $\theta^\delta_{\beta,0}(t)$ (blue-dash line) in Fig. 3(c), respectively. It is shown that the evolution of $|\lambda_{\beta,0}\rangle$ is non-adiabatic, and the non-adiabatic phase correction is non-negligible. Thus the GAA breaks down, and the calculation based on the adiabatic LIP model can not reproduce the spectral lineshape well, as presented in Fig. 3(f). It is also shown that, the calculation based on the TDGF approach reproduces the spectral lineshape in the TDSE-RK calculation well in the region of the $1s^2$–$1s2p$ resonant absorption peak and the low-frequency sideband, but not in the region of the high-frequency sideband. As only the dipole transition between $|\lambda_{\beta,0}\rangle$ and $|\lambda_{\alpha,0}\rangle$ is included in the Floquet calculation, i.e., Eqs. (22) and (19), one can deduce that this disagreement in the high-frequency sideband is due to the neglect of Floquet states that are populated by the IR pulse. Our TDGF calculation indicates that a non-negligible population is excited from $|\lambda_{\beta,0}\rangle$ to $|\lambda_{\gamma,1}\rangle$ owing to the non-adiabatic near-resonant coupling driven by the IR pulse, as shown with the black-dash-dotted line in Fig. 3(c). We rewrite Eqs. (18) and (19), to include the dipole transition between $|\lambda_{\gamma,1}\rangle$ and $|\lambda_{\alpha,0}\rangle$, as

$$S'_F(\omega) = 2\tilde{\varepsilon}_X \mathrm{Im}[\tilde{d}'_F(\omega)] \tag{24}$$

with

$$\tilde{d_{\rm F}^{\gamma}}(\omega) = {\rm i}a_{\rm X}\int_{\tau}^{\infty}\left[a^{\delta}_{\beta,0}(t)\mu_{\beta\alpha}\,{\rm e}^{-{\rm i}\theta^{\rm T}_{\beta,0}(t)}\,{\rm e}^{{\rm i}[\omega-\omega_{\beta\alpha})t} + a^{\delta}_{\gamma,1}(t)\mu_{\gamma\alpha}\,{\rm e}^{-{\rm i}\theta^{\rm T}_{\gamma,1}(t)}\,{\rm e}^{{\rm i}(\omega-\omega_{\gamma\alpha})t}\right]W(t)\,{\rm d}t. \quad (25)$$

With the improved version of TDGF calculation, Eqs. (24) and (25), we obtain the spectral lineshape which agrees well with the TDSE-RK calculation in the regions of both the absorption peak and sidebands, as presented with the red-dash-dotted line in Fig. 3(f). The result based on the RWA calculation including both $|\lambda_{\beta,0}\rangle$ and $|\lambda_{\gamma,1}\rangle$ agrees well with both the TDSE-RK and the improved TDGF calculations. It is implied that the first-order Floquet quasienergy vectors are the major components of the Floquet states $|\lambda_{\beta,0}\rangle$ and $|\lambda_{\gamma,1}\rangle$, and the non-adiabatic near-resonant IR-coupling between adiabatic Floquet states is captured in the RWA.

3.4. Comparison with *ab initio* calculation

Although the above investigations are just with a primitive two-level model, we confirm the efficiency of the TDGF approach via the comparison with the *ab initio* calculation of the SAE helium atom (see Appendix A for details) in the three cases. As presented by Fig. 5, the TDGF calculation (red-dotted line) is different from the *ab initio* calculation (black-solid line). The difference is due to the ionization and the multi-level effect in real atomic systems. The lack of multi-level effect can be improved by including more levels in the TDGF calculation. The TDGF calculation with 11-level model, including 1s2s–1s4s, 1s2p–1s5p and 1s3d–1s6d, is plotted in Fig. 5 with the blue-dash line, presenting quite good agreement with the *ab initio* calculation.

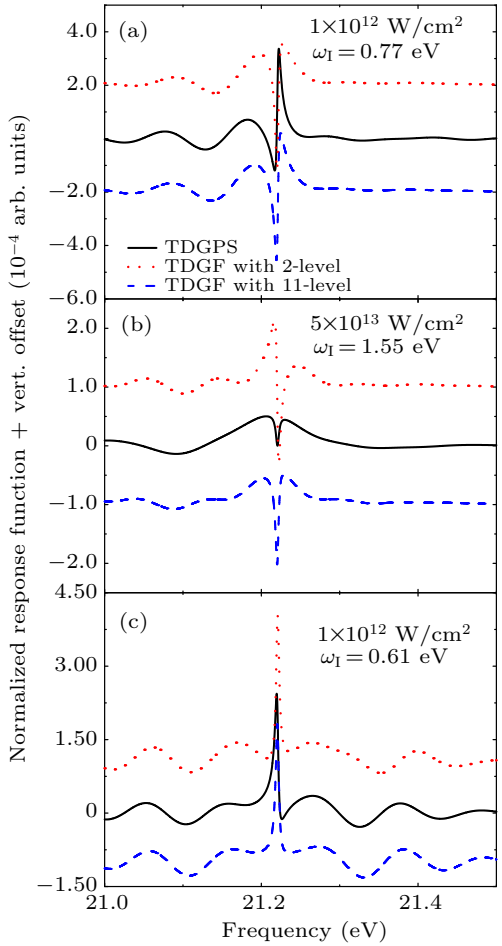


Fig. 5. The comparison of response functions based on different approaches in the cases with (a) $I_{\rm IR} = 1\times10^{12}$ W/cm^2 and $\omega_{\rm I} = 0.77$ eV, (b) $I_{\rm IR} = 5\times10^{13}$ W/cm^2 and $\omega_{\rm I} = 1.55$ eV, and (c) $I_{\rm IR} = 1\times10^{12}$ W/cm^2 and $\omega_{\rm I} = 0.61$ eV. The TDGPS calculation is plotted with black-solid line, and the TDGF calculations with 2-level and 11-level models are plotted with red-dotted and blue-dash lines, respectively.

4. Conclusion

In this paper, we introduce an alternative numerical approach, the time-dependent generalized Floquet (TDGF) approach, to calculate the ATA spectra of a helium atomic system driven by the combination of an attosecond XUV pulse and a delayed few-cycle IR pulse. An additional understanding of the laser-induced lineshape change in ATA spectra is provided in the framework of adiabatic Floquet states.

In terms of adiabatic Floquet states, we derive the total phase shift imported on the time-dependent dipole moment, and demonstrate the adiabatic LIP and the non-adiabatic phase correction, by employing the generalized adiabatic theorem. The comparisons with the RWA and the adiabatic LIP model are presented in three typical cases. All three approaches agree well with the numerical RK calculation in the case of weak driving and moderate detuning. The adiabatic LIP model fails in the case of weak driving and small detuning, due to the non-adiabatic near-resonant cross-coupling between adiabatic Floquet states. While the RWA fails in the case of strong driving and large detuning, because the higher-order Floquet quasienergy vectors that are coupled in the formation of adiabatic Floquet states, i.e., the rotating-wave terms, are dropped off in the RWA. Although the numerical results in this paper are calculated in the three-level model, a better agreement with the *ab initio* calculation can be obtained by employing the model including more energy levels. We expect that the following approach will enable the direct experimental observation of lineshape changes induced by the non-adiabatic phase: Tune the gradients of the pulse envelope, by changing the pulse durations and peak intensities of IR pulses, to control the non-adiabatic phase, and keep the dynamical phase shifts unchanged by maintaining the areas of the IR pulses.

Appendix A: The *ab initio* simulation

Under the SAE approximation, the TDSE describing the interaction of a single He atom with laser field can be written as

$${\rm i}\frac{\partial}{\partial t}|\Psi(\boldsymbol{r},t)\rangle = \hat{H}(t)|\Psi(\boldsymbol{r},t)\rangle = [\hat{H}_0+\hat{V}(t)]|\Psi(\boldsymbol{r},t)\rangle. \quad (A1)$$

Here the laser–atom interaction within the dipole approximation is given by

$$\hat{V}(t) = -\boldsymbol{E}(t)\cdot\boldsymbol{r}, \tag{A2}$$

and $\hat{H}_0$ represents the unperturbed atom Hamiltonian, which can be written as

$$\hat{H}_0 = -\frac{1}{2}\nabla^2 + \sum_l |Y_l^0\rangle V_l \langle Y_l^0|, \tag{A3}$$

where V_l is model potential for He atom, and Y_l^0 is a spherical harmonic. We employ an angular-momentum-dependent model potential in the following form:

$$V_l = \frac{\alpha}{2r^4} W_6\left(\frac{r}{r_c}\right) - \frac{1}{r} - \left(\frac{N-S}{r} + A_1\right) e^{-B_1 r} - \left(\frac{S}{r} + A_2\right) e^{-B_2 r}, \tag{A4}$$

where α is the He^+ core dipole polarizability.[45,46] W_6 is a core cutoff function given bey

$$W_n(x) = 1 - \left[1 + nx + \frac{(nx)^2}{2!} + \cdots + \frac{(nx)^2}{n!}\right] e^{-nx}, \tag{A5}$$

and r_c is an effective He^+ core radius. The values of the parameters determined are listed in Table A1. In the present work, it is sufficient to use four different angular-momentum-dependent model potentials.

Table A1. Model potential parameters for He (in a.u.).

l	α	r_c	S	A_1	A_2	B_1	B_2
0	0.28125	2.0	–7.9093912	–10.899664	0.0	1.7	3.8
1	0.28125	2.0	1.50094970	0.11297684	0.0	1.3	3.8
2	0.28125	2.0	0.88294766	–0.032043029	0.0	1.3	3.8
3	0.28125	2.0	0.41193110	–0.129391180	0.0	1.3	3.8
> 3	0.28125	2.0	0.0	0.0	0.0	1.3	0.0

Via the diagonalization of the field-free Hamiltonian $\hat{H}_0$, one can obtain the eigenstates of the SAE He atom, and the transition matrix elements between them. The TDSE can be solved numerically by means of the time-dependent generalized pseudospectral (TDGPS) method.[47] The maximum radius of the grid is set at $r_{max} = 150$, and the number of collocation points along the radial coordinate is $N_r = 300$. The absorbing boundary starting at $r_b = 100$ is employed to avoid the artificial reflection. The pulse-envelope function is Gaussian shaped and centered around $t = 0$ for the IR and τ for the XUV, respectively. After the time propagation of the wavefunction $\Psi(\boldsymbol{r},t)$, we can calculate the expectation value of the induced dipole moment in the length,

$$d(t) = \langle \Psi(\boldsymbol{r},t)|z|\Psi(\boldsymbol{r},t)\rangle. \tag{A6}$$

And the absorption spectra can be obtained via substituting the Fourier transformation of Eq. (A6) multiplied with the decaying function Eq. (4) into the response function Eq. (6).

Acknowledgement

Project supported by the National Natural Science Foundation of China (Grant Nos. W2411002 and 12375018).

References

[1] Goulielmakis E, Loh Z H, Wirth A, Santra R, Rohringer N, Yakovlev V S, Zherebtsov S, Pfeifer T, Azzeer A M, Kling M F, Leone S R and Krausz F 2010 *Nature* **466** 739
[2] Chew A, Douguet N, Cariker C, Li J, Lindroth E, Ren X, Yin Y, Argenti L, Hill W T and Chang Z 2018 *Phys. Rev. A* **97** 031407
[3] Cao W, Warrick E R, Neumark D M and Leone S R 2016 *New J. Phys.* **18** 013041
[4] Wang X, Chini M, Cheng Y, Wu Y, Tong X M and Chang Z 2013 *Phys. Rev. A* **87** 063413
[5] Kaldun A, Blättermann A, Stooß V, Donsa S, Wei H, Pazourek R, Nagele S, Ott C, Lin C D, Burgdörfer J and Pfeifer T 2016 *Science* **354** 738
[6] Chini M, Zhao B, Wang H, Cheng Y, Hu S X and Chang Z 2012 *Phys. Rev. Lett.* **109** 073601
[7] Chen S, Schafer K J and Gaarde M B 2012 *Opt. Lett.* **37** 2211
[8] Holler M, Schapper F, Gallmann L and Keller U 2011 *Phys. Rev. Lett.* **106** 123601
[9] Sabbar M, Timmers H, Chen Y J, Pymer A K, Loh Z H, Sayres S G, Pabst S, Santra R and Leone S R 2017 *Nat. Phys.* **13** 472
[10] Ott C, Kaldun A, Raith P, Meyer K, Laux M, Evers J, Keitel C H, Greene C H and Pfeifer T 2013 *Science* **340** 716
[11] Ott C, Kaldun A, Argenti L, Raith P, Meyer K, Laux M, Zhang Y, Blättermann A, Hagstotz S, Ding T, Heck R, Madroñero J, Martín F, Pfeifer T 2014 *Nature* **516** 374
[12] Bækhøj J E, Lévêque C and Madsen L B 2018 *Phys. Rev. Lett.* **121** 023203
[13] Rørstad J J, Ravn N S W, Yue L and Madsen L B 2018 *Phys. Rev. A* **98** 053401
[14] Warrick E R, Bækhøj J E, Cao W, Fidler A P, Jensen F, Madsen L B, Leone S R and Neumark D M 2017 *Chem. Phys. Lett.* **683** 408
[15] Cheng Y, Chini M, Wang X, González-Castrillo A, Palacios A, Argenti L, Martín F and Chang Z 2016 *Phys. Rev. A* **94** 023403
[16] Liao C T, Li X, Haxton D J, Rescigno T N, Lucchese R R, McCurdy C W and Sandhu A 2017 *Phys. Rev. A* **95** 043427
[17] Bækhøj J E, Yue L, Madsen L B 2015 *Phys. Rev. A* **91** 043408
[18] Garg M, Martin-Jimenez A, Pisarra M, Luo Y, Martín F and Kern K 2021 *Nat. Photon.* **16** 196
[19] Golubev N V, Vaníček J and Kuleff A I 2021 *Phys. Rev. Lett.* **127** 123001
[20] Shi X, Wu Y, Wang J, Kimberg V and Zhang S 2020 *Phys. Rev. A* **101** 023401
[21] Schultze M, Ramasesha K, Pemmaraju C, Sato S, Whitmore D, Gandman A, Prell J S, Borja L J, Prendergast D, Yabana K, Neumark D M and Leone S R 2014 *Science* **346** 1348
[22] Lucchini M, Sato S A, Ludwig A, Herrmann J, Volkov M, Kasmi L, Shinohara Y, Yabana K, Gallmann L and Keller U 2016 *Science* **353** 916
[23] Moulet A, Bertrand J B, Klostermann T, Guggenmos A, Karpowicz N and Goulielmakis E 2017 *Science* **357** 1134
[24] Seres E, Seres J, Serrat C and Namba S 2016 *Phys. Rev. B* **94** 165125
[25] Hui D, Alqattan H, Yamada S, Pervak V, Yabana K and Hassan M Th 2021 *Nat. Photon.* **16** 33
[26] Géneaux R, Kaplan C J, Yue L, Ross A D, Bækhøj J E, Kraus P M, Chang H T, Guggenmos A, Huang M Y, Zürch M, Schafer K J, Neumark D M, Gaarde M B and Leone S R 2020 *Phys. Rev. Lett.* **124** 207401
[27] Liu Z, Wang F, Sheng X, Wang J, Jiang L and Wei Z 2021 *Phys. Rev. B* **104** 064103
[28] Krausz F and Ivanov M 2009 *Rev. Mod. Phys.* **81** 163
[29] Calegari F, Sansone G, Stagira S, Vozzi C and NIsoli M 2016 *J. Phys. B* **49** 062001
[30] Bengtsson S, Larsen E W, Kroon D, Camp S, Miranda M, Arnold C L, L'Huillier A, Schafer K J, Gaarde M B, Rippe L, *et al.* 2017 *Nat. Photonics* **11** 252
[31] Corkum P B and Krausz F 2007 *Nat. Phys.* **3** 381

[32] Gallmann L, Cirelli C and Keller U 2012 *Annu. Rev. Phys. Chem.* **63** 447

[33] Yuan G, Jiang S, Wang Z, Hua W, Yu C, Jin C and Lu R 2019 *Struct. Dyn.* **6** 054102

[34] Rørstad J J, Bækhøj J E and Madsen L B 2017 *Phys. Rev. A* **96** 013430

[35] Wu M, Chen S, Camp S, Schafer K J and Gaarde M B 2016 *J. Phys. B* **49** 062003

[36] Reduzzi M, Hummert J, Dubrouil A, Calegari F, Nisoli F, Frassetto F, Poletto L, Chen S, Wu M, Gaarde M B, Schafer K and Sansone G 2015 *Phys. Rev. A* **92** 033408

[37] Chini M, Wang X, Cheng Y, Wu Y, Zhao D, Telnov D A, Chu S I and Chang Z 2013 *Sci. Rep.* **3** 1105

[38] Chen S, Wu M, Gaarde M B and Schafer K J 2013 *Phys. Rev. A* **88** 033409

[39] Stooß V, Cavaletto S M, Donsa S, Blättermann A, Birk P, Keitel C H, Březinová I, Burgdörfer J, Ott C and Pfeifer T 2018 *Phys. Rev. Lett.* **121** 173005

[40] Liu Z, Ott C, Cavaletto S M, Harman Z, Keitel C H and Pfeifer T 2014 *New J. Phys.* **16** 093005

[41] Dodin A and Brumer P 2021 *PRX Quantum* **2** 030302

[42] Gaarde M B, Buth C, Tate J L and Schafer K J 2011 *Phys. Rev. A* **83** 013419

[43] Chen S, Bell M J, Beck A R, Mashiko H, Wu M, Pfeiffer A N, Gaarde M B, Neumark D M, Leone S R and Schafer K J 2012 *Phys. Rev. A* **86** 063408

[44] Chu S I and Telnov D A 2004 *Phys. Rep.* **390** 1

[45] Li P C, Laughlin C and Chu S I 2014 *Phys. Rev. A* **89** 023431

[46] Chu X, Chu S I and Laughlin C 2001 *Phys. Rev. A* **64** 013406

[47] Tong X M and Chu S I 1997 *Chem. Phys.* **217** 119